Journal of Electronic Materials, Vol. 21, No. 12, 1992

Properties and Use of $In_{0.5}(Al_xGa_{1-x})_{0.5}P$ and $Al_xGa_{1-x}As$ Native Oxides in Heterostructure Lasers

F. A. KISH,[a] S. J. CARACCI, N. HOLONYAK, JR., K. C. HSIEH, J. E. BAKER, S. A. MARANOWSKI, A. R. SUGG and J. M. DALLESASSE[b]

Electrical Engineering Research Laboratory, Center for Compound Semiconductor Microelectronics, and Materials Research Laboratory, University of Illinois at Urbana-Champaign, Urbana, Illinois 61801

R. M. FLETCHER, C. P. KUO, T. D. OSENTOWSKI and M. G. CRAFORD

Hewlett-Packard Company, Optoelectronics Division, San Jose, California 95131

Data are presented demonstrating the formation of native oxides from high Al composition $In_{0.5}(Al_xGa_{1-x})_{0.5}P$ ($x \geq 0.9$) by simple annealing in a "wet" ambient. The oxidation occurs by reaction of the high Al composition crystal with H_2O vapor (in a N_2 carrier gas) at elevated temperatures (≥500° C) and results in stable transparent oxides. Secondary ion mass spectrometry (SIMS) as well as scanning and transmission electron microscopy (SEM and TEM) are employed to evaluate the oxide properties, composition, and oxide-semiconductor interface. The properties of native oxides of the $In_{0.5}(Al_xGa_{1-x})_{0.5}P$ system are compared to those of the $Al_xGa_{1-x}As$ system. Possible reaction mechanisms and oxidation kinetics are considered. The $In_{0.5}(Al_xGa_{1-x})_{0.5}P$ native oxide is shown to be of sufficient quality to be employed in the fabrication of stripe-geometry $In_{0.5}(Al_xGa_{1-x})_{0.5}P$ visible-spectrum laser diodes.

Key words: $In_{0.5}(Al_xGa_{1-x})_{0.5}P$, $Al_xGa_{1-x}As$, native oxides, III–V native oxides, Al-bearing III–V oxides, III–V "wet" oxidation, oxide-defined heterostructure lasers

INTRODUCTION

The modern electronics revolution has been primarily a result of the advancement of Si integrated circuit (IC) technology. While the discovery of the point contact transistor by Bardeen and Brattain[1] was probably the most significant development leading to this technology, much of the Si IC development relies critically on the ability to form high-quality, dense, stable, and insulating native oxides on Si. The discovery that such an oxide (SiO_2) could be formed on Si by H_2O vapor oxidation[2] continues to be of major significance. Attempts to form similar high-quality native oxides on III–V semiconductor compounds have met with limited success.[3] In general, these oxides have poor electrical and/or mechanical properties, and are porous, making them unable to mask impurity diffusion. This inability to form high-quality native oxides on the III–V compounds has impeded the development of III–V IC and optoelectronic technology.

Recently, in attempts to study the degradation of high-gap $Al_xGa_{1-x}As$,[4,5] stable device-quality insulating AlGaAs native oxides have been realized.[6] These oxides are formed in a manner similar to the classical method of oxidizing Si,[2] by reaction of high-gap $Al_xGa_{1-x}As$ with H_2O vapor (in a N_2 carrier gas) at elevated temperatures (≥400° C).[6] The high-quality of the native oxides is attributed to the formation of stable AlO(OH) and Al_2O_3 compounds, in marked contrast to $Al(OH)_3$ and related compounds that are believed to be formed in room-temperature destructive atmospheric hydrolysis.[7] Thus, the key to the formation of the high-quality III–V oxides is the presence of Al in the semiconductor. Hence, any III–V with sufficient Al composition, *i.e.* $In_{0.5}(Al_xGa_{1-x})_{0.5}P$,[8] may be employed to form these high-quality oxides. The $Al_xGa_{1-x}As$ native oxides are dense, and have been shown to mask Zn (acceptor) diffusion (and impurity induced layer disordering (IILD)) from the vapor (600° C),[9] and Si (donor) solid-source diffusion and IILD (800° C).[10] The excellent insulating characteristics of the native oxide make it useful for the fabrication of high-performance gain-guided $Al_xGa_{1-x}As$ lasers.[11,12] Furthermore, the native oxide is capable of reducing leakage currents from parasitic *p-n* shunt junctions, resulting in an improved form of IILD buried heterostructure laser.[13] The $Al_xGa_{1-x}As$ native oxides also exhibit a low refractive index ($n \sim 1.60$) and can be made thick (microns), making them useful in forming essentially planar index-guided lasers,[14,15] and planar optical waveguides with large bend angles.[16] In addition, the low-index oxides can be employed to form internal reflectors for Fabry-Perot cavities.[17]

In view of the above, the native oxide has already proven to be an extremely useful fabrication technology for the realization of optoelectronic devices. In order to fully realize the potential of the Al-bearing III–V native oxides, a detailed understanding of the oxide material properties and oxidation processes is required. In this paper, we present data on

a) AT&T Doctoral Fellow. Now at Hewlett-Packard Co., Optoelectronics Division, San Jose, California 95131.

b) Now at Amoco Techn. Co., Amoco Research Ctr., Naperville, Illinois 60566.

(Received June 15, 1992)

0361-5235/1992/1401-1133$5.00©92 TMS

the properties of oxides formed from high Al composition $In_{0.5}(Al_xGa_{1-x})_{0.5}P$ ($x \geq 0.9$) and $Al_xGa_{1-x}As$ ($x \geq 0.5$). Transmission and scanning electron microscopy (TEM and SEM) and secondary ion mass spectroscopy (SIMS) are utilized to investigate and compare the properties of $In_{0.5}(Al_xGa_{1-x})_{0.5}P$ and $Al_xGa_{1-x}As$ native oxides. Possible reaction mechanisms, oxidation chemistry and growth kinetics are discussed. In addition, applications of the In(AlGa)P native oxide to the fabrication of stripe-geometry $In_{0.5}(Al_xGa_{1-x})_{0.5}P$ visible-spectrum laser diodes are presented.

EXPERIMENTAL PROCEDURE

The crystals employed in this work are grown on (100) GaAs substrates by metalorganic chemical vapor deposition (MOCVD).[18] The primary source materials consist of trimethylgallium, trimethylaluminum, trimethylindium, phosphine, and arsine. Bulk layers of $Al_xGa_{1-x}As$ ($x \geq 0.5$) and $In_{0.5}(Al_xGa_{1-x})_{0.5}P$ ($x \geq 0.9$) have been investigated for material characterization studies. In addition, a double heterostructure (DH) laser designed for $\lambda \sim$ 665 nm emission is also employed. The crystal is grown on an *n*-type GaAs substrate with a ~0.8 μm $In_{0.5}(Al_{0.9}Ga_{0.1})_{0.5}P$ *n*-type lower confining layer, a ~0.1 μm undoped $In_{0.5}Ga_{0.5}P$ active region, a ~0.8 μm $In_{0.5}(Al_{0.9}Ga_{0.1})_{0.5}P$ *p*-type upper confining layer, and a ~200Å $In_{0.5}Ga_{0.5}P$ *p*-type contact layer.

"Wet" oxidations are conducted in an open-tube furnace (400–650° C) supplied with H_2O vapor. The H_2O vapor is supplied via an N_2 carrier gas passed through a H_2O bubbler maintained at ~95° C. The total N_2 flow rate is 1.4 scfh. This experimental arrangement results in saturation of the N_2 with H_2O vapor. It is not essential to heat the lines between the bubbler and furnace to avoid condensation. Generally, this process results in the formation of high quality native oxides from both $Al_xGa_{1-x}As$ and $In_{0.5}(Al_xGa_{1-x})_{0.5}P$. We note that attempts to form native oxides from high Al composition $Al_xGa_{1-x}As$ with O_2 gas results in lower quality oxides, with a decreased amount of oxygen present in the films compared to those formed with H_2O vapor.[19]

Various methods are employed to characterize the native oxide and underlying semiconductor crystal. Secondary ion mass spectrometry (SIMS) measurements are performed with a Cameca IMS 3F ion microprobe with primary beam of Cs+ ions and positive secondary ion detection. All SIMS ion counts are normalized to give the proper stoichiometric ratio in the semiconductor crystal. Samples are prepared for transmission electron microscopy (TEM) by cleaving the wafers into small rectangles (2 × 2 mm), mounting pairs face-to-face with epoxy, sawing the sandwiched pair into ~0.25 mm bars, and Ar^+ ion milling the samples to the required thickness. TEM images are generated on a Phillips EM 420 microscope. Oxide depth measurements are performed by cleaving, staining, and imaging oxide-semiconductor cross sections in a scanning electron microscope (SEM). Stains consisting of $HCl:H_2O_2:H_2O$ (1:4:40) and Br-methanol (0.1%) are employed to delineate the oxide.

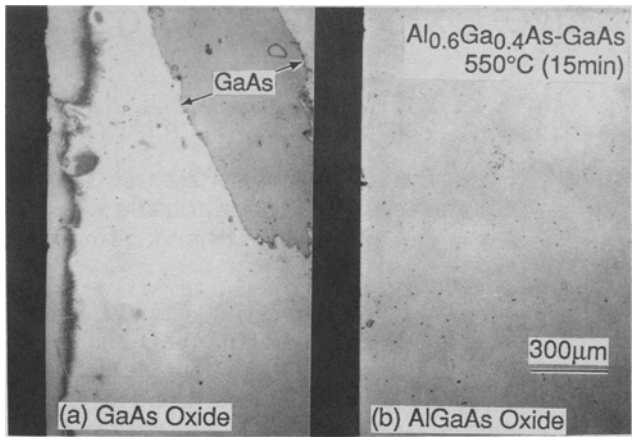

Fig. 1 — Optical micrographs of oxide films formed from (a) GaAs and (b) $Al_{0.6}Ga_{0.4}As$ via H_2O vapor oxidation at 550° C for 15 min. The oxide formed from the GaAs is not mechanically stable and can easily be removed by applying pressure with a small wooden stylus (upper right, in (a)). In contrast, (b) the AlGaAs oxide is mechanically very stable and cannot be removed even with considerable force.

RESULTS AND DISCUSSION

The oxides formed by "wet" oxidation from the Al-bearing III–V's exhibit markedly different properties than those formed from III–V compounds that do not contain Al. Figure 1 shows optical micrographs of the surface of oxides formed simultaneously from (a) GaAs and (b) $Al_{0.6}Ga_{0.4}As$ at 550° C for 15 min. The GaAs oxide (~0.2 μm) is not mechanically stable and can be easily removed from the underlying GaAs by applying pressure with a small wooden stylus (upper right corner of Fig. 1(a)). However, the oxide formed from $Al_{0.6}Ga_{0.4}As$ (~0.3 μm thick) is mechanically very stable and cannot be removed even with considerable force. Oxides ~2 μm thick have been formed from high-gap $Al_xGa_{1-x}As$ which exhibit excellent mechanical, insulating, and diffusion masking properties (data not shown).

The high quality of the Al-bearing oxides is attributed to the properties of Al within the oxide. The oxidation potential (defined as the potential for the removal of three electrons from the Column III metal, $III \rightarrow III^{3+} + 3e^-$) of Al (+1.66) is much higher than that of Ga (+0.53) or In (+0.34).[20] Thus, Al-bearing compounds oxidize more readily as a result of the high affinity of Al for oxygen (or OH, H_2O) molecules. The direct consequence of this property is a reduced amount of unoxidized metal (Al) in the oxide (compared to oxides formed from Ga or In), resulting in a film with improved insulating and mechanical properties.

The high affinity of Al for oxygen results in the Al composition (mole fraction) of AlGaAs being a key rate determining factor in the growth of Al-

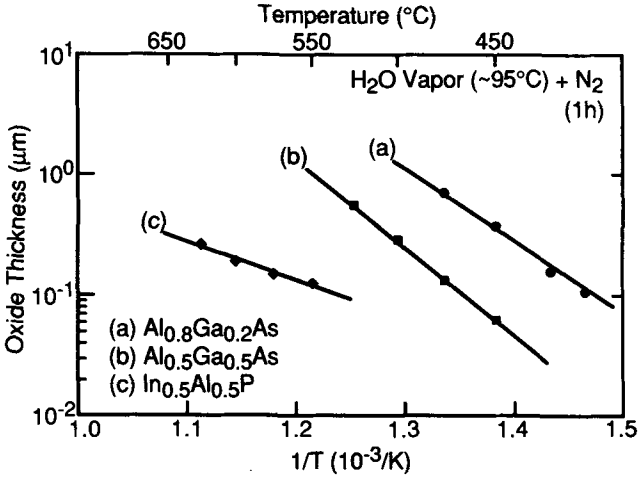

Fig. 2 — Oxide thickness vs inverse temperature (1/T) for the H_2O vapor oxidation (1h) of (a) $Al_{0.8}Ga_{0.2}As$, (b) $Al_{0.5}Ga_{0.5}As$, and (c) $In_{0.5}Al_{0.5}P$. The higher Al content of the (a) $Al_{0.8}Ga_{0.2}As$ results in an increased oxidation rate compared to lower Al-content (b) $Al_{0.5}Ga_{0.5}As$. However, for samples containing the same Al mole fraction, (b) $Al_{0.5}Ga_{0.5}As$ oxidizes more rapidly than (c) $In_{0.5}Ga_{0.5}P$.

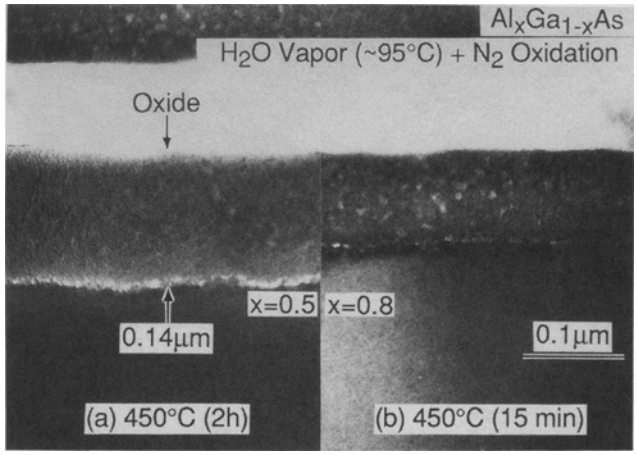

Fig. 3 — Transmission electron microscope images of native oxides formed via H_2O vapor oxidation at 450° C from (a) $Al_{0.5}Ga_{0.5}As$ (2h) and (b) $Al_{0.8}Ga_{0.2}As$ (15 min). The structure of both oxides is the same, essentially amorphous, with a moderately smooth interface at the oxide-semiconductor boundary. The crystalline granules observed inside the oxide are most likely the result of electron beam irradiation and are not inherently present in the oxide.

GaAs native oxide films by water vapor oxidation. This trend is shown in the Fig. 2 plot of oxide thickness vs inverse temperature (1/T) for lh "wet" oxidations of (a) $Al_{0.8}Ga_{0.2}As$ and (b) $Al_{0.5}Ga_{0.5}As$. Both samples are doped *p*-type mid-10^{17} cm^{-3} to eliminate any doping level influence on the oxidation growth rate.[21] For all temperatures investigated, the higher Al-composition AlGaAs oxidizes "faster" than AlGaAs of lower Al-composition. In addition, the slope of the oxide thickness vs (1/T) curve in Fig. 2 is steeper for (b) $Al_{0.5}Ga_{0.5}As$ than (a) $Al_{0.8}Ga_{0.2}As$, which implies a higher activation energy for the oxidation of lower Al-composition AlGaAs in Fig. 2(b). The results are a consequence of the reduced amount of Al present to absorb (or chemisorb) the oxygen-containing molecules in order to initiate the oxidation process.

The presence of Al is the key to forming high quality oxides from the III–V compounds by "wet" oxidation. Thus, other III–V semiconductors containing a sufficient amount of Al are also candidates for conversion to high quality native oxides. Specifically, the $In_{0.5}(Al_xGa_{1-x})_{0.5}P$ system may be employed to form device-quality oxides.[8] In Fig. 2, the results for oxide thickness vs (1/T) are also presented for the "wet" oxidation of (c) $In_{0.5}Al_{0.5}P$ (*p*-type mid-10^{17} cm^{-3}). These data indicate that $In_{0.5}Al_{0.5}P$ oxidizes at a much slower rate compared to $Al_{0.5}Ga_{0.5}As$ (both compounds containing the same mole fraction of Al and same doping level). Also, higher temperatures (≥500° C) are required to form oxides from $In_{0.5}Al_{0.5}P$ compared to $Al_{0.5}Ga_{0.5}As$, which oxidizes at substantially lower temperatures (≥450° C). These higher oxidation temperatures result in a decreased selectivity between the oxidation rates for $In_{0.5}(Al_xGa_{1-x})_{0.5}P$ and III–V compounds which do not contain Al. Thus, $In_{0.5}Ga_{0.5}P$ or GaAs *do not* serve as appropriate masks for the oxidation of $In_{0.5}(Al_xGa_{1-x})_{0.5}P$. For water vapor oxidations performed at 500° C (4h), TEM measurements indicate the formation of ~200Å of oxide on exposed $In_{0.5}Ga_{0.5}P$ surfaces (data not shown). This behavior is unlike that of the oxidation of $Al_xGa_{1-x}As$ which under the appropriate conditions may be masked by thin GaAs capping layers.[12,13]

The slope of the oxide depth vs (1/T) curve of Fig. 2 implies a much lower activation energy for the (c) $In_{0.5}Al_{0.5}P$ compared to (b) $Al_{0.5}Ga_{0.5}As$. The reduced activation energy may be a consequence of the presence of "soft" In-P crystal bonds that are more easily broken compared to those of Ga-As or Al-As. The dissociation of these bonds may be a limiting step in the oxidation process[3] resulting in a lower activation energy for $In_{0.5}Al_{0.5}P$ (compared to $Al_{0.5}Ga_{0.5}As$).

Figure 3 shows TEM images of oxides formed by water vapor oxidation (450° C) of (a) $Al_{0.5}Ga_{0.5}As$ (2h) and (b) $Al_{0.8}Ga_{0.2}As$ (15 min). In both cases the native oxide is essentially amorphous with a moderately smooth interface at the oxide-semiconductor boundary. No discernible differences are present in the structure of the two oxides. However, these images indicate the presence of small crystalline granules within the native oxide. We note that the structural changes shown in Fig. 3 develop in an otherwise uniform oxide film only after prolonged electron beam irradiation. Thus, these crystalline granules are most likely a result of radiation damage and are *not* inherently present in the oxide. Similar results have been observed for Al_2O_3, where amorphous material recrystallizes after irradiation by a focused electron beam.[22]

The smoothness of the boundary at the AlGaAs native oxide-semiconductor interface may be improved by employing $In_{0.5}Ga_{0.5}P$-$In_{0.5}(Al_xGa_{1-x})_{0.5}P$ "stop-layers". These phosphorus compounds oxidize at a much slower rate, and thus effectively serve to

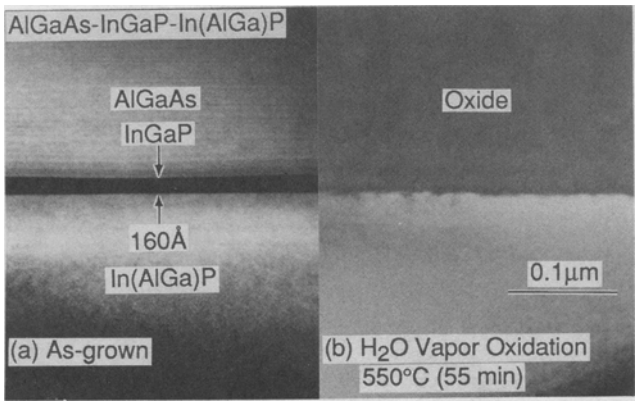

Fig. 4 — Transmission electron microscope image of an (a) as-grown AlGaAs-InGaP-In(AlGa)P heterostructure in which the InGaP-In(AlGa)P layers are employed to terminate (stop) the oxidation of the upper AlGaAs layer. After oxidation (550° C, 55 min) the image in (b) indicates that the InGaP layer is "consumed", with the oxide terminating within the In(AlGa)P layer. The oxide-semiconductor boundary exhibits a much smoother interface than that of the oxidation of bulk AlGaAs (Fig. 3).

"stop" the oxidation process under the proper conditions. A structure employing such stop-layers is shown in the TEM image of Fig. 4(a). The layers of interest consist of ~0.3 μm $In_{0.5}(Al_{0.9}Ga_{0.1})_{0.5}P$, and ~160Å $In_{0.5}Ga_{0.5}P$ capped with a ~0.5 μm $Al_{0.4}Ga_{0.6}As$ oxidation layer. Such structures can be advantageously employed to form planar index-guided visible-spectrum laser diodes via the water vapor oxidation process.[23] The effect of the stop-layers is shown in Fig. 4(b) where the surface of the crystal ($Al_{0.4}Ga_{0.6}As$ layer) has been exposed to H_2O vapor at 550° C for 55 min. The oxidation process results in the conversion of the entire ~0.5 μm $Al_{0.4}Ga_{0.6}As$ layer to native oxide. In addition, the ~160Å $In_{0.5}Ga_{0.5}P$ layer is consumed in the process. At 550° C, the entire $Al_{0.4}Ga_{0.6}As$ layer is consumed after ~37 min. The much slower oxidation rates of the $In_{0.5}(Al_xGa_{1-x})_{0.5}P$ compounds serve to "stop" the oxidation process at this point. No further oxidation of the underlying $In_{0.5}(Al_xGa_{1-x})_{0.5}P$ layer is observed for all longer oxidation times investigated (≤90 min). We note that the AlGaAs-oxide semiconductor interface is significantly smoother when oxidation "stop-layers" are employed (Fig. 4(b)) compared to the oxidation of bulk AlGaAs layers (Fig. 3).

The water vapor oxidation of bulk high Al-composition $In_{0.5}(Al_xGa_{1-x})_{0.5}P$ also results in a relatively smooth oxide-semiconductor interface (compared to the oxidation of bulk AlGaAs, Fig. 3). This is shown in the TEM images of Fig. 5 for the "wet" oxidation of $In_{0.5}(Al_xGa_{1-x})_{0.5}P$ at (a) 500° C (4h), (b) 550° C (1h), and (c) 650° C (12 min). Under all conditions investigated the oxide film is essentially amorphous. However, small crystalline islands are also observed in these films (Fig. 5). Similar to the crystalline granules observed in the AlGaAs oxide (Fig. 3), these crystalline islands are most likely an artifact of the electron beam irradiation of the sample and are *not* an intrinsic property of the oxide. Also, such islands may result from the Ar+ ion milling process as has been previously observed in InP.[24]

The concentration of the crystalline islands does reflect, however, the distribution of In within the oxide. Thus, for $In_{0.5}(Al_xGa_{1-x})_{0.5}P$ oxidized at (a) 500° C (4h) an accumulation of islands (In) occurs at the oxide-semiconductor interface, whereas at (b) 550° C (1h) the islands (In) appear to be relatively uniformly distributed within the oxide. At (c) 650° C (12 min), a depletion of islands (In) exists at the interface. The correlation of island concentration with In distribution is confirmed by the SIMS In profiles of these samples shown in Fig. 6. In agreement with the TEM images, the SIMS profiles show an In accumulation at (a) 550° C (4h) and an In depletion at (c) 650° C (12 min) occurring at the oxide-semiconductor interface (~0.1 μm in depth from the surface). The SIMS In profile at (b) 550° C roughly shows an even distribution of In within the oxide film. SIMS signals for the other elements (Al, Ga, O, H) show no differences for films formed at different temperatures (data not shown). Thus, the oxidation temperature significantly affects the In distribution within the oxide.

These results, of course, have implications for the formation of thick oxide films from $In_{0.5}(Al_xGa_{1-x})_{0.5}P$. At temperatures ≥575° C, H_2O vapor oxidation results in poor quality non-uniform films for oxides thicker than ~3000Å. These films typically have a silver appearance which is attributed to the migration of In toward the surface. However, for H_2O vapor oxidation at 550° C, we have successfully fabricated thick films (~0.7 μm). These films appear to be of high-quality, with a smooth oxide-semiconductor interface. Similar to AlGaAs oxide, depth (x_j) vs time (t) measurements for $In_{0.5}(Al_xGa_{1-x})_{0.5}P$ oxidized at 550° C indicate that the oxidation growth rate conforms to a parabolic law ($x_j^2 \propto t$, data not shown) indicating the formation of a protective, nonporous film.[21] This behavior is unlike that for films formed according to a linear oxidation growth rate ($x_j \propto t$). Such films are generally regarded as porous since the growth rate does not decrease with oxide thickness, indicating that the oxidizing species pass unimpeded through the film.

Secondary ion mass spectrometry data for films formed by "wet" oxidation from $Al_{0.5}Ga_{0.5}As$ at 450° C for 2h are shown in Fig. 7. These data indicate a chemically sharp interface (within the resolution of the SIMS sputtering) between the oxide and the $Al_{0.5}Ga_{0.5}As$. As expected, a significant amount of O and H is present in the oxide. The same results are observed for oxides formed from higher composition $Al_xGa_{1-x}As$, *i.e.* $x \sim 0.8$ (data not shown). We note that the exact chemical composition of these films cannot presently be determined from these data due to matrix effects and the lack of standards. In addition, SIMS data are shown in Fig. 8 for an oxide formed from $In_{0.5}(Al_{0.9}Ga_{0.1})_{0.5}P$ at 500° C for 4h. Similar to the oxides formed from $Al_xGa_{1-x}As$ (Fig. 7), the In(AlGa)P oxide exhibits a chemically sharp interface and the presence of a substantial amount of O and H in the oxide. However, these data (Fig.

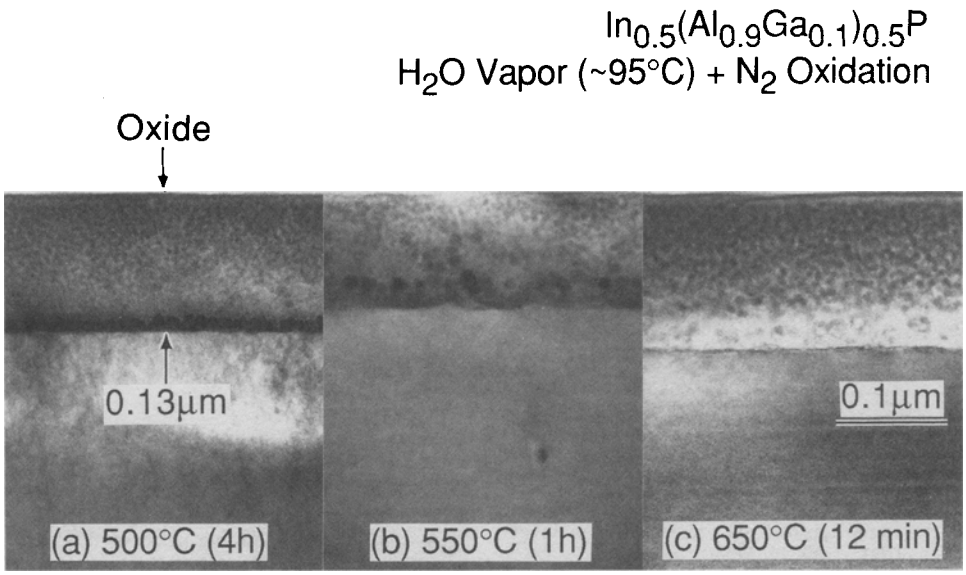

Fig. 5 — Transmission electron microscope images of oxides formed from $In_{0.5}(Al_{0.9}Ga_{0.1})_{0.5}P$ via "wet" oxidation at (a) 500° C (4h), (b) 550° C (1h), and (c) 650° C (12 min). The oxide structure is essentially amorphous with a significantly smoother oxide-semiconductor interface compared to oxides formed from bulk AlGaAs (Fig. 3). The crystalline islands shown in these images are a result of radiation damage from the TEM and are not an intrinsic property of the oxide. However, these islands reflect the In distribution within the film, indicating an In accumulation at the oxide-semiconductor interface at (a) 550° C, and an In depletion from the interface at (c) 650° C. At (b) 550° C, the islands (In) are roughly evenly distributed throughout the oxide.

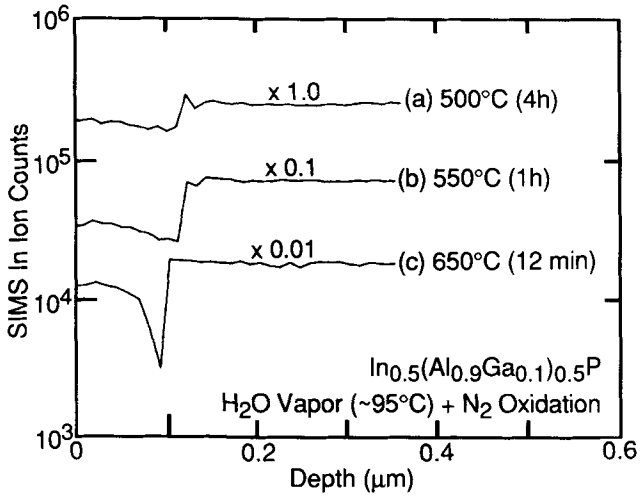

Fig. 6 — SIMS In profiles of the In(AlGa)P oxide films of Fig. 5 formed by H_2O vapor oxidation at (a) 500° C (4h), (b) 550° C (1h), and (c) 650° C (12 min). The In profiles agree with the observed distribution of crystalline islands in the TEM images of Fig. 5. These data indicate an accumulation at (a) 500° C, and a depletion at (c) 650° C of In from the oxide-semiconductor interface (~0.1 μm in depth). The SIMS profile for (b) 550° C shows a relatively uniform In distribution throughout the oxide.

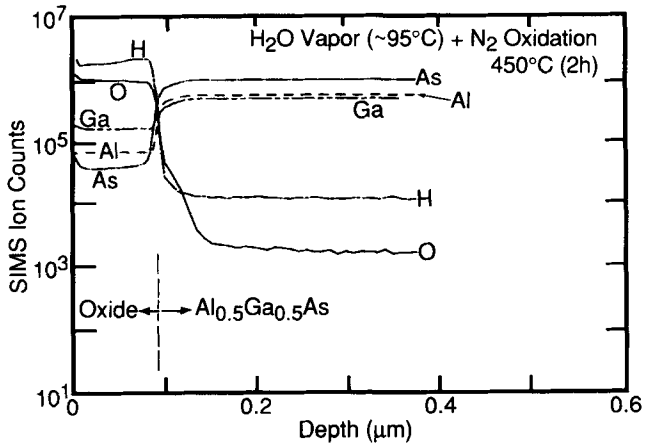

Fig. 7 — SIMS profiles for the water vapor oxidation (450° C, 2h) of $Al_{0.5}Ga_{0.5}As$. The oxide contains a significant amount of O and H and exhibits a chemically sharp interface with the underlying $Al_{0.5}Ga_{0.5}As$ (within the SIMS sputtering resolution).

8) indicate a significantly lower concentration of H (compared to that of O) in the In(AlGa)P oxide. These results are in contrast to those obtained from the AlGaAs oxide (Fig. 7) which indicate the presence of more H than O in the oxide. This phenomenon may be a consequence of either variation in the oxidation chemistry resulting from the presence of In/P, or the higher temperature required for the oxidation of $In_{0.5}(Al_{0.9}Ga_{0.1})_{0.5}P$ (500° C) compared to $Al_{0.5}Ga_{0.5}As$ (450° C). Such a higher temperature may cause a different oxide compound and/or phase to be formed (*e.g.* more Al_2O_3 than AlO(OH)).

The presence of *some* (≤ 50% mole fraction) Ga in the native oxide films of Figs. 7 and 8 does not compromise the structural integrity of the film. The reaction products for the high-temperature H_2O vapor oxidation of AlAs are thought to be AlO(OH) and/or Al_2O_3.[7] The oxides of Ga, GaO(OH) and Ga_2O_3, and Al, AlO(OH) and Al_2O_3, are structural isomorphs, and thus form an extended series of solid solutions, $Al_xGa_{1-x}O(OH)$ and $(Al_xGa_{1-x})_2O_3$, over virtually their entire composition range.[25-27] However, the In oxide compounds exhibit a much more limited range of solid solubility with the oxides of Al and Ga.[27,28] This property combined with the high

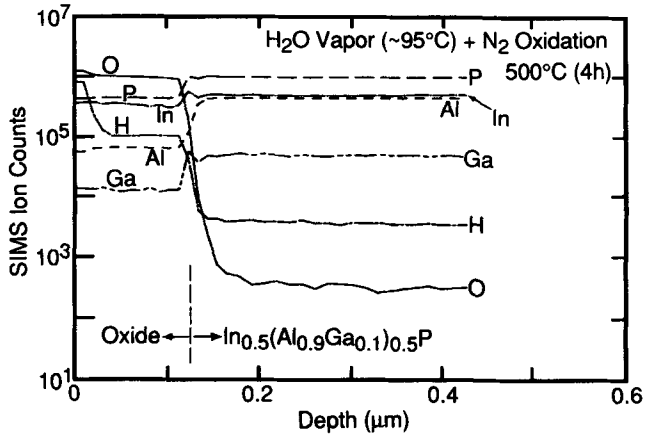

Fig. 8 — SIMS profiles for the 500° C (4h) H_2O vapor oxidation of $In_{0.5}(Al_{0.9}Ga_{0.1})_{0.5}P$. These profiles are similar to those of AlGaAs oxides (Fig. 7), with the exception of a significantly lower level of H (compared to that of O) in the In(AlGa)P oxide.

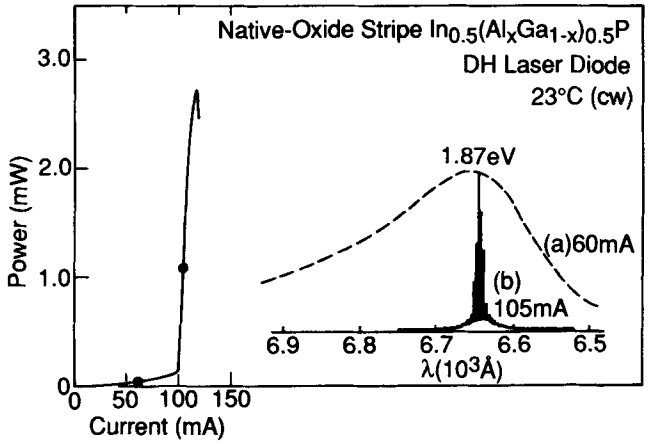

Fig. 9 — Continuous (cw) room-temperature (23° C) performance characteristics of 10-μm-wide gain-guided native-oxide-defined $In_{0.5}(Al_xGa_{1-x})_{0.5}P$ double heterostructure laser diode. The laser has a threshold of 98 mA (2.6 kA/cm^2) and operates in multiple longitudinal modes at $\lambda \sim 665$ nm (inset). The laser exhibits a maximum power output of 2.75 mW/facet (uncoated) with a total external differential quantum efficiency of 27%.

diffusivity of In may account for the temperature dependence of the In distribution in the oxide film (Figs. 5 and 6). The Column V elements may also oxidize, forming As_2O_3 or P_2O_5 (which is thermodynamically more stable than P_2O_3).[3] Both of these compounds possess a very high vapor pressure and thus tend to evaporate from the oxide.[3] Additionally, the P or As may react with H to form AsH_3(g) and PH_3(g). These mechanisms indicate that a reduced amount of the Column V element should be present in the oxide.

Despite the mixed composition of the oxide films, both the AlGaAs oxide[11] and the In(AlGa)P oxide[8] exhibit excellent insulating characteristics. Also, ellipsometer measurements (λ = 632.8 nm), indicate that the AlGaAs oxide possesses a refractive index of $n \sim 1.6$.[19] Ellipsometer measurements indicate that the In(AlGa)P oxides also exhibit a refractive index of $n \sim 1.6$, which is relatively independent of the oxidation temperature (500–650° C). The low index of these native oxides may be advantageously employed for optical confinement in the higher index ($n \sim 3$) semiconductor material.

The In(AlGa)P native oxide is of sufficient quality, exhibiting very good insulating characteristics, to be employed for current confinement in the fabrication of $In_{0.5}(Al_xGa_{1-x})_{0.5}P$ gain-guided laser diodes. Devices are fabricated by patterning 10-μm-wide Si_3N_4 stripes on the crystal surface which are then employed as masking layers to chemically etch the contact layer, thus exposing the high Al composition $In_{0.5}(Al_xGa_{1-x})_{0.5}P$ upper confining layer outside of the stripe region. The crystals are then immediately placed in an open tube furnace (500–550° C) supplied with H_2O vapor in an N_2 carrier gas for 1–4h. This process transforms the surface of the exposed $In_{0.5}(Al_xGa_{1-x})_{0.5}P$ confining layer to a ~1000Å current-blocking native oxide. The Si_3N_4 masking stripes are then selectively removed, and the sample is lapped and polished to ~125 μm, metallized with Au-Zn-Au for p-type contacts and Ge-Ni-Au for n-type contacts, cleaved, diced, and mounted on In-coated copper heat sinks.

The continuous (cw) room-temperature (23° C) light vs current (L-I) characteristics of a 10-μm-wide device fabricated from the DH visible-spectrum laser crystal are shown in Fig. 9. The laser threshold is 98 mA (2.6 kA/cm^2) with a total external differential quantum efficiency (η) of 27%. The maximum power output is limited to 2.75 mW/facet (uncoated). The device exhibits a fairly high characteristic temperature (T_o) for this material system of 125° C under pulsed operation and 100° C under cw operation. The laser operates in multiple longitudinal modes at $\lambda \sim 665$ nm (inset). We note that the operating characteristics of these devices defined by the native oxide are comparable to (are at least as good as) those defined by deposited dielectrics (Si_3N_4 or SiO_2). Laser diode performance in this material system is typically limited by thermal considerations as a result of the high electrical and thermal resistivity of the $In_{0.5}(Al_xGa_{1-x})_{0.5}P$ confining layers. The native oxide devices may ultimately yield improved thermal performance as a result of the superior adherence of the native oxide film and the excellent thermal properties of Al_2O_3.

CONCLUSIONS

Data have been presented describing the material properties of native oxides formed via H_2O vapor oxidation from high Al composition AlGaAs and In(AlGa)P. The Al content of the samples is shown to critically affect the oxidation rate. However, the presence of In and/or P significantly slows the oxidation process. Accordingly, In(AlGa)P layers can be employed as "stop-layers" for the oxidation of AlGaAs. Both the AlGaAs oxides and In(AlGa)P oxides are amorphous in structure. However, the In distribution within the native oxide is highly dependent on the oxidation temperature. Under the proper conditions, the In distribution can be made

uniform, allowing the formation of thick oxide films. Furthermore, the In(AlGa)P native oxide possesses excellent insulating characteristics (and a low refractive index) and thus can be advantageously employed in the fabrication of $In_{0.5}(Al_xGa_{1-x})_{0.5}P$ laser diodes.

ACKNOWLEDGMENTS

The authors are grateful to E. I. Chen, (Urbana) for contributions to this work and S. C. Smith and R. D. Burnham (Amoco) for providing some comparison AlGaAs crystals. For technical assistance, the authors wish to thank B. L. Payne and R. T. Gladin. The work of the Illinois group has been supported by Army Research Office Contract DAAL 03-89-K-0008, and National Science Foundation Grants ECD 89-43166 and DMR 89-20538.

REFERENCES

1. J. Bardeen and W. H. Brattain, Phys. Rev. *74*, 230 (1948).
2. C. J. Frosch and L. Derick, J. Electrochem. Soc. *104*, 547 (1957); see also, C. J. Frosch, "Silicon Diffusion Technology," in Transistor Technology, ed. F. J. Biondi (Van Nostrand, Princeton, NJ, 1958), Vol. *3*, pp. 90–99.
3. C. W. Wilmsen, Thin Solid Films *39*, 105 (1976).
4. J. M. Dallesasse, P. Gavrilovic, N. Holonyak, Jr., R. W. Kaliski, D. W. Nam, E. J. Vesely and R. D. Burnham, Appl. Phys. Lett. *56*, 2436 (1990).
5. J. M. Dallesasse, N. El-Zein, N. Holonyak, Jr., K. C. Hsieh, R. D. Burnham and R. D. Dupuis, J. Appl. Phys. *68*, 2235 (1990).
6. J. M. Dallesasse, N. Holonyak, Jr., A. R. Sugg, T. A. Richard and N. El-Zein, Appl. Phys. Lett. *57*, 2844 (1990).
7. A. R. Sugg, N. Holonyak, Jr., J. E. Baker, F. A. Kish and J. M. Dallesasse, Appl. Phys. Lett. *58*, 1199 (1991).
8. F. A. Kish, S. J. Caracci, N. Holonyak, Jr., A. R. Sugg, R. M. Fletcher, C. P. Kuo, T. D. Osentowski and M. G. Craford, Appl. Phys. Lett. *59*, 354 (1991).
9. J. M. Dallesasse, N. Holonyak, Jr., N. El-Zein, T. A. Richard, F. A. Kish, A. R. Sugg, R. D. Burnham and S. C. Smith, Appl. Phys. Lett. *58*, 974 (1991).
10. N. El-Zein, N. Holonyak, Jr., F. A. Kish, A. R. Sugg, T. A. Richard, J. M. Dallesasse, S. C. Smith and R. D. Burnham, J. Appl. Phys. *70*, 2031 (1991).
11. J. M. Dallesasse and N. Holonyak, Jr., Appl. Phys. Lett. *58*, 394 (1991).
12. J. M. Dallesasse N. Holonyak, Jr., D. C. Hall, N. El-Zein, A. R. Sugg, S. C. Smith and R. D. Burnham, Appl. Phys. Lett. *58*, 834 (1991).
13. F. A. Kish, S. J. Caracci, N. Holonyak, Jr., J. M. Dallesasse, G. E. Höfler, R. D. Burnham and S. C. Smith, Appl. Phys. Lett. *58*, 1765 (1991).
14. F. A. Kish, S. J. Caracci, N. Holonyak, Jr., J. M. Dallesasse, K. C. Hsieh, M. J. Ries, S. C. Smith and R. D. Burnham, Appl. Phys. Lett. *59*, 1755 (1991).
15. F. A. Kish, S. J. Caracci, N. Holonyak, Jr., P. Gavrilovic, K. Meehan and J. E. Williams, Appl. Phys. Lett. *60*, 71 (1992).
16. F. A. Kish, S. J. Caracci, S. A. Maranowski, N. Holonyak, Jr., S. C. Smith and R. D. Burnham, Appl. Phys. Lett. *60*, 1582 (1992).
17. N. El-Zein, F. A. Kish, N. Holonyak, Jr., A. R. Sugg, M. J. Ries, S. C. Smith, J. M. Dallesasse and R. D. Burnham, Appl. Phys. Lett. *59*, 2838 (1991).
18. R. D. Dupuis, L. A. Moudy and P. D. Dapkus, in Proc. of the Int. Symp. on GaAs and Related Compounds, ed. C. M. Wolfe (Institute of Physics, London, 1979), pp. 1–9; see also
    M. J. Ludowise, J. Appl. Phys. *58*, R31 (1985).
19. A. R. Sugg, E. I. Chen and N. Holonyak, Jr., unpublished data.
20. C. D. Hodgman, Handbook of Chemistry and Physics, (Chemical Rubber Co., Cleveland, Ohio, 1961), p. 1740.
21. F. A. Kish, S. A. Maranowski, G. E. Höfler, N. Holonyak, Jr., S. J. Caracci, J. M. Dallesasse and K. C. Hsieh, Appl. Phys. Lett. *60*, 3165 (1992).
22. P. S. Sklad, Proc. of the Electron Microscopy Soc. of America, ed. G. W. Bailey (San Francisco Press, San Francisco, 1986), pp. 508–511.
23. F. A. Kish, S. J. Caracci, S. A. Maranowski, N. Holonyak, Jr., K. C. Hsieh, C. P. Kuo, R. M. Fletcher, T. D. Osentowski and M. G. Craford, J. Appl. Phys. *71*, 2521 (1992).
24. N. G. Chew and A. G. Cullis, Appl. Phys. Lett. *44*, 142 (1984).
25. F. A. Cotton and G. Wilkinson, Advanced Inorganic Chemistry (Wiley, New York, 1966), pp. 439–440.
26. J. A. Kohn, G. Katz and J. D. Broder, Am. Mineral. *42*, 398 (1957).
27. E. M. Levin, C. R. Robbins and H. F. McMurdie, Phase Diagrams for Ceramists, ed. M. K. Reser (American Ceramic Society, Columbus, 1964), pp. 121–122, 134.
28. J. C. Bailar, Jr., H. F. Emeleus, Ronald Nyholm and H. F. Trotman-Dickenson Comprehensive Inorganic Chemistry (Pergamon Press, New York, 1973), pp. 1093–1094.